$4^{th}$ **International Conference on**
**Earthquake Geotechnical Engineering**
June 25-28, 2007
Paper No. 1623

# A NEW FAST BEM APPROACH TO MODEL SITE EFFECTS IN ALLUVIAL BASINS

**Stéphanie CHAILLAT** [1] , **Marc BONNET** [2] , **Jean-François SEMBLAT** [3]

## ABSTRACT

The solution of the elastodynamic equations using integral formulations requires to solve full and non symmetric systems. The use of an iterative solver like GMRES lowers the complexity of the solution (number of operations) to order $N^2$, where $N$ is the number of degrees of freedom (DOFs). The most expensive computational task is the matrix-vector product. For Helmholtz and Maxwell equations, the fast multipole method (FMM) is known to dramatically reduce that cost. This is achieved by (i) using a *multipole expansion* of the relevant Green's tensor, which allows to reuse element integrals for all collocation points, and (ii) defining a (recursive, multi-level) partition of the region of space enclosing the domain boundary of interest into cubic cells, allowing to optimally cluster influence computations. Moreover, the matrix of the system is not stored with the FMM. So, the complexity (both in CPU time and memory) is found to be $N \log_2 N$ per iteration. The fast multipole formulation of the boundary element method for 3D elastodynamics in frequency domain is presented in this article. Numerical efficiency and accuracy are assessed on the basis of numerical results obtained for problems having known solutions. Finally, the present FMM-BEM is demonstrated on seismology-oriented examples, namely the study of the diffraction of a plane wave or a point source by a canyon. The influence of the size of the meshed part of the free surface is studied, and computations are performed for non-dimensional frequencies higher than those considered in other studies, with which comparisons are made whenever possible.

Keywords: site effects, boundary element method, seismic wave amplification, 3D, Fast Multipole Method.

## INTRODUCTION

Seismic site effects are a major concern for earthquake engineering because very large local amplifications of seismic motions may occur. Such phenomena can strengthen the surface ground motion and increase the consequences on structures and buildings. To analyze site effects, it is possible to consider modal approaches (Semblat et al., 2003) or directly investigate wave propagation phenomena (Bard and Bouchon, 1985; Semblat et al., 2005). The importance of 2D and 3D simulations is well recognized throughout the literature. A lot of studies have been devoted to the 2D case. The 3D case is currently

[1]PhD Student, Laboratoire de Mécanique des Solides, École Polytechnique, France, Email: chaillat@lms.polytechnique.fr
[1]& Laboratoire Central des Ponts et Chaussées, Paris, France
[2]Senior scientist, Laboratoire de Mécanique des Solides, École Polytechnique, France
[3]Senior scientist, Laboratoire Central des Ponts et Chaussées, Paris, France

a very attractive field of research because of the increase of the speed and capabilities of computers. To compute seismic wave propagation in alluvial basins, various numerical methods have been proposed (Semblat and Bard, 2005): the series expansions (Lee, 1984), the multipolar expansions of wave functions (Sánchez-Sesma, 1983), the finite element method, the finite differences, the spectral elements method (Chaljub et al., 2003), the boundary element method (BEM, see e.g. Bonnet, 1999; Dangla et al., 2005; Guzina and Pak, 2001). The main advantage of the latter is that only the domain boundaries (and possibly interfaces) are discretized, leading to a reduction of the number of degrees of freedom (DOFs). However, the standard BEM leads to fully-populated, non-symmetric matrices. This entails high computational costs, both in CPU time ($O(N^2)$ per iteration using an iterative solver such as GMRES) and memory requirements ($O(N^2)$), where $N$ denotes the number of DOFs of the BEM model.

In other research areas where the BEM is used (electromagnetism, acoustics,...), considerable speedup of solution time and decrease of memory requirements has been achieved, over the last decade, through the development of the Fast Multipole Method (FMM) (Nishimura, 2002). This method is known to reduce the CPU time to $O(N \log_2 N)$ per iteration. So far, very few studies have been devoted to the FMM in elastodynamics (see, however, Fujiwara (2000) for the frequency-domain case and Takahashi et al. (2003) for the time-domain case). The present article improves on the methodology of (Fujiwara, 2000) by incorporating recent advances of FMM implementations for Maxwell equations (e.g. Darve (2000)), which allow to run BEM models of much larger size.This paper is organized as follows. First, the main features of the elastodynamic FMM-BEM formulation are concisely presented. Then, numerical efficiency and accuracy are assessed on numerical results obtained for problems with well-known solutions. Finally, the efficiency of the present FMM-BEM is demonstrated on seismology-oriented examples.

## BOUNDARY INTEGRAL METHOD

### Boundary integral representation

In this study, only isotropic linear elasticity is considered, in the frequency-domain ($\omega$ denoting the circular frequency). The material constants are : the mass-density $\rho$, the shear modulus $\mu$ and the Poisson's ratio $\nu$. The Maxwell-Betti reciprocity identity applied to two states, namely the sought (unknown) elastodynamic solution over an elastic body $\Omega$ and the full-space Green's tensor, leads (assuming no body forces) to the well-known boundary integral identity (e.g. Bonnet, 1999):

$$\kappa u_k(\boldsymbol{x}) = \int_{\partial\Omega} [t_i(\boldsymbol{y}) U_i^k(\boldsymbol{x},\boldsymbol{y};\omega) - u_i(\boldsymbol{y}) T_i^k(\boldsymbol{x},\boldsymbol{y};\omega)] dS_y, \tag{1}$$

with $\kappa = 1$ if $\boldsymbol{x} \in \Omega$ and $\kappa = 0$ if $\boldsymbol{x} \notin \bar{\Omega}$, and where $U_i^k(\boldsymbol{x},\boldsymbol{y};\omega)$ and $T_i^k(\boldsymbol{x},\boldsymbol{y};\omega)$ denote the $i$-th component of the displacement and traction, respectively, generated at $\boldsymbol{y} \in \mathbb{R}^3$ by a unit point force applied at $\boldsymbol{x} \in \mathbb{R}^3$ along direction $k$. $\boldsymbol{U}(\boldsymbol{x},\boldsymbol{y};\omega)$ is hence the full-space Green's tensor, also known as elastodynamic fundamental solution. Equation (1) holds only if $\boldsymbol{x} \notin \partial\Omega$.

The full-space elastodynamic Green's tensor is given by (Eringen and Suhubi, 1975):

$$\begin{aligned} U_i^k(\boldsymbol{x},\boldsymbol{y};\omega) &= \frac{1}{4\pi k_S^2 \mu}\Big((\delta_{qs}\delta_{ik} - \delta_{qk}\delta_{is})\frac{\partial}{\partial x_q}\frac{\partial}{\partial y_s} G_S(|\boldsymbol{y}-\boldsymbol{x}|) + \frac{\partial}{\partial x_i}\frac{\partial}{\partial y_k} G_P(|\boldsymbol{y}-\boldsymbol{x}|)\Big), \\ T_i^k(\boldsymbol{x},\boldsymbol{y};\omega) &= C_{ijh\ell}\frac{\partial}{\partial y_\ell} U_h^k(\boldsymbol{x},\boldsymbol{y};\omega) n_j(\boldsymbol{y}), \end{aligned} \tag{2}$$

where $G_\alpha(|\boldsymbol{y}-\boldsymbol{x}|)$ is the free-space Green's function for the Helmholtz equation with wavenumber $k_\alpha$,

$$G_\alpha(|\boldsymbol{y}-\boldsymbol{x}|) = \frac{\exp(ik_\alpha|\boldsymbol{y}-\boldsymbol{x}|)}{|\boldsymbol{y}-\boldsymbol{x}|} \qquad (\alpha = S, P), \tag{3}$$

$k_S$ and $k_P$ denote the wavenumbers of the $S$ and $P$ waves, $C_{ijh\ell}$ are the components of the (isotropic) elastic tensor and $\boldsymbol{n}(\boldsymbol{y})$ is the unit normal to $\partial\Omega$ directed outwards of $\Omega$.

**Boundary integral equations**

When $\boldsymbol{x} \in \partial\Omega$, a singularity occurs in $\boldsymbol{y} = \boldsymbol{x}$. The counterpart of integral identity (1) for the case $\boldsymbol{x} \in \partial\Omega$ is obtained by performing a limiting process. This well-documented step leads to the integral equation:

$$c_{ik}(\boldsymbol{x})u_i(\boldsymbol{x}) = \text{(P.V.)} \int_{\partial\Omega} [t_i(\boldsymbol{y})U_i^k(\boldsymbol{x},\boldsymbol{y};\omega) - u_i(\boldsymbol{y})T_i^k(\boldsymbol{x},\boldsymbol{y};\omega)]dS_y, \tag{4}$$

where (P.V.) $\int$ indicates a Cauchy principal value (CPV) singular integral and $c_{ik}(\boldsymbol{x})$, called the free term, is equal to $0.5\delta_{ik}$ in the usual case where $\partial\Omega$ is smooth at $\boldsymbol{x}$. Alternatively, equation (4) may be recast into equivalent regularized forms which are free of CPV integrals.

## FAST MULTIPOLE METHOD: PRINCIPLE

**One-level algorithm**

The boundary element method entails the solution of a linear system, whose governing matrix is fully-populated and unsymmetric. The solution step may be performed using either direct solvers (typically based on a LU factorization) or iterative solvers (typically GMRES). The solution time is $O(N^3)$ for the former, and $O(N^2)$ per iteration for the latter. Since the overall number of iterations is usually much smaller than $N$, iterative solvers are preferable for large BEM models. Each iteration of GMRES requires the computation of one matrix-vector product, hence the $O(N^2)$ computing time since the matrix is full. The goal of the FMM is to speed up the matrix-vector product computation. Moreover, the governing matrix is never explicitly formed, which leads to a storage requirement well below the $O(N^2)$ memory that would be needed for holding the complete matrix. The FMM-accelerated BEM, described next, therefore achieves substantial savings in both CPU time and memory.

In general terms, the main idea behind the FMM is to reformulate the fundamental solutions in terms of products of functions of $\boldsymbol{x}$ and of $\boldsymbol{y}$. This allows to reuse integrations with respect to $\boldsymbol{y}$ when the collocation point $\boldsymbol{x}$ is changed, a strategy which is not feasible in the traditional BEM, based on expressions (2). The latter are seen to be linear combinations of the Green's function for the Helmholtz equation (3), for which such a reformulation is known from earlier works in acoustics and electromagnetism. Denoting by $\boldsymbol{r} = |\boldsymbol{y} - \boldsymbol{x}|$ the position vector, it can be decomposed as $\boldsymbol{r} = (\boldsymbol{x_0} - \boldsymbol{x}) + (\boldsymbol{y_0} - \boldsymbol{x_0}) - (\boldsymbol{y_0} - \boldsymbol{y}) = \tilde{\boldsymbol{x}} + \boldsymbol{r_0} - \tilde{\boldsymbol{y}}$, where $\boldsymbol{x_0}$ and $\boldsymbol{y_0}$ are two poles. Application of the Gegenbauer addition theorem (Abramowitz and Stegun, 1992) permits to write the Helmholtz Green's function as

$$\frac{\exp(ik|\boldsymbol{y} - \boldsymbol{x}|)}{|\boldsymbol{y} - \boldsymbol{x}|} = \frac{ik}{4\pi} \lim_{L\to+\infty} \int_{\tilde{\boldsymbol{s}}\in S} e^{ik\tilde{\boldsymbol{s}}.\tilde{\boldsymbol{x}}} \mathcal{G}_L(\tilde{\boldsymbol{s}}; \boldsymbol{r_0}) e^{-ik\tilde{\boldsymbol{s}}.\tilde{\boldsymbol{y}}} d\tilde{\boldsymbol{s}}, \tag{5}$$

where

$$\mathcal{G}_L(\tilde{\boldsymbol{s}}; \boldsymbol{r_0}) = \sum_{0\le l\le L} (2l+1) i^\ell h_\ell^{(1)}(k|\boldsymbol{r_0}|) P_\ell\big(\cos(\tilde{\boldsymbol{s}}, \boldsymbol{r_0})\big) \tag{6}$$

is the *transfer function*, $S$ is the unit sphere of $\mathbb{R}^3$, $\tilde{\boldsymbol{s}}$ is a point on $S$ (i.e. a unit vector), $P_\ell$ is the Legendre polynomial of order $l$, and $h_\ell^{(1)}$ is the spherical Hankel function of first kind and order $\ell$. Then, the elastodynamic fundamental solution (2) is easily seen to admit representations of the form (5) with $\mathcal{G}_L$ replaced with suitably-defined (tensor) transfer functions $\mathcal{U}_{i,L}^{\alpha,k}$ and $\mathcal{T}_{i,L}^{\alpha,k}$ ($\alpha = S, P$).

Formula (5) with $L = O(k_S|\boldsymbol{r} - \boldsymbol{r_0}|)$ is suitably accurate whenever $|\boldsymbol{r} - \boldsymbol{r_0}|/|\boldsymbol{r_0}| \le 2/\sqrt{5}$ Darve (2000). Guided by this consideration, a 3D cubic grid of linear spacing $d$, containing the whole boundary $\partial\Omega$, is introduced (Figure 1). The above condition is then verified any time $\boldsymbol{x}$ and $\boldsymbol{y}$ belong to non-adjacent cubic cells, the poles $\boldsymbol{x_0}$ and $\boldsymbol{y_0}$ being chosen as the cell centers, but may be violated when $\boldsymbol{x}$

and $\boldsymbol{y}$ belong to adjacent cubic cells. The one-level FMM basically consists of using decomposition (5) whenever $\boldsymbol{x}$ and $\boldsymbol{y}$ belong to non-adjacent cells, while staying with the traditional expression (3) if $\boldsymbol{x}$ and $\boldsymbol{y}$ belong to adjacent cells.

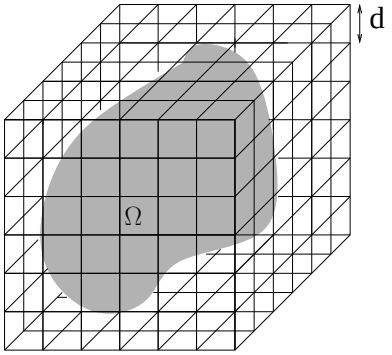


**Figure 1**: **Cubical decomposition of the domain in 3D**

A typical contribution of this kind to the residual of (1) or (4) is of the form:

$$I_k(\boldsymbol{x}) = \int_{\partial\Omega\cap\mathcal{C}_y} t_i(\boldsymbol{y}) U_i^k(\boldsymbol{x},\boldsymbol{y},\omega) dS_y \qquad (\boldsymbol{x}\in\mathcal{C}_x)$$

where $\mathcal{C}_x$ and $\mathcal{C}_y$ denote cubic cells with respective centers $\boldsymbol{x_0}$ and $\boldsymbol{y_0}$ (which are used as poles in decomposition (5)) and $\boldsymbol{t}$ is associated to a solution candidate. On inserting (5), for a well-chosen finite $L$, into (2), $I_k(\boldsymbol{x})$ is evaluated by means of a three-step computational procedure which is summarized by ($\alpha = S, P$) :

$$\mathcal{R}_i^\alpha(\tilde{\boldsymbol{s}}_q;\boldsymbol{y_0}) = \int_{\partial\Omega\cap\mathcal{C}_y} t_i(\boldsymbol{y_0}+\tilde{\boldsymbol{y}}) e^{-ik_\alpha \tilde{\boldsymbol{s}}_q.\tilde{\boldsymbol{y}}} dS_{\tilde{y}} \qquad \text{computation of multipole moments} \qquad (7)$$

$$\mathcal{L}_k^\alpha(\tilde{\boldsymbol{s}}_q;\boldsymbol{x_0}) = \mathcal{U}_{i,L}^{\alpha,k}(\tilde{\boldsymbol{s}}_q;\boldsymbol{r_0})\mathcal{R}_i^\alpha(\tilde{\boldsymbol{s}}_q;\boldsymbol{y_0}) \qquad \text{transfer} \qquad (8)$$

$$I_k^\alpha(\boldsymbol{x}) \approx \sum_q w_q \frac{ik_\alpha}{4\pi} e^{ik_\alpha \tilde{\boldsymbol{s}}_q.\tilde{\boldsymbol{x}}} \mathcal{L}_k^\alpha(\tilde{\boldsymbol{s}}_q;\boldsymbol{x_0}) \qquad \text{local expansion} \qquad (9)$$

where $\tilde{\boldsymbol{s}}_q$ and $w_q$ are quadrature points and weights for the integration over the unit sphere. When cells $\mathcal{C}_x$ and $\mathcal{C}_y$ are adjacent, traditional BEM evaluation methods based on expressions (2) and (3) are used.

The one-level fast multipole method in the elastodynamics case has an optimal complexity of $O(N^{3/2})$. This complexity is achieved by using $O(N^{3/4})$ cells. It is already more efficient than the classical BEM, but the multi-level algorithm provides further acceleration.

**Multi-level algorithm**

The method is based on an idea reminiscent of the sorting algorithm known as *quicksort*, which consists in recursively dividing the table being sorted into two subtables and perform the sorting on the two subtables. Similarly, optimal acceleration of the BEM is achieved by confining standard (i.e. non-FMM) calculations to the smallest possible spatial regions.

Because the series (5) needs to be truncated at a suitable level, the FMM can only be applied for two non-adjacent cells. For instance, with reference to Figure 2 (left), integrals arising from the FMM and performed over boundary elements located in the dark-gray cell (including e.g. node $j$) can be used only for collocation points lying in white cells (e.g. node 3). To reduce the size of the spatial region (here, the light-grey cells adjacent to the dark-gray one) where the FMM decomposition is not applicable, a natural idea is to subdivide the current cells (say, of level 0) into smaller cells (say, of level 1), and

possibly repeat the process (levels 2, 3, ...). In Figure 2 (right), this new level allows to apply the FMM treatment for all collocation points lying in the hatched cells (including e.g. node 2), while the adjacent, non-FMM region (light-grey, including e.g. node 1) reduces in size. Summing up, the FMM is first applied, whenever possible, to all interactions at level 0, to maximize CPU efficiency afforded by clustering. Then, the FMM is applied at level 1 to all interactions between disjoint cells (at that level) which could not be treated at level 0.

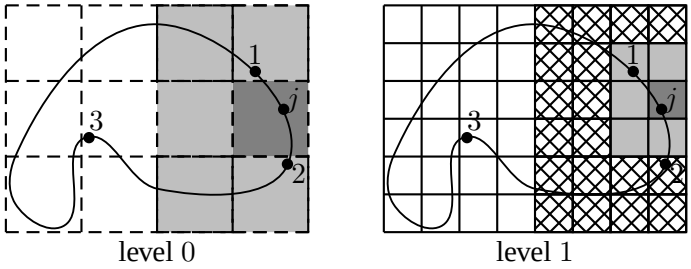


**Figure 2**: **Optimal choice of the level for the FMM computation of the matrix-vector product**

The previously outlined method is a two-level FMM. The same approach can be generalized to several levels of nested cubic cells. A very important consideration is that, for a given desired accuracy, the truncation parameter $L$ in the transfer function (6) is level-dependent, and increases with the cell-size-to-wavelength ratio. Because of that consideration, the theoretical complexity of the multi-level FMM is $O(N \log_2 N)$ per iteration both for CPU time and memory (i.e. somewhat higher than the $O(N)$ complexity for static FMM-BEM, where the truncation parameter in the FMM expansion is not level-dependent).

## FAST MULTIPOLE METHOD: ACCURACY AND COMPUTATIONAL EFFICIENCY

### Spherical cavity under internal pressure

A spherical cavity of radius $R$ embedded in an elastic isotropic infinite space (with Poisson's ratio $0.25$) and subjected to an internal pressure $P(\omega)$ (Figure 3). This problem has a simple, spherically-symmetric, exact solution (Eringen and Suhubi, 1975) given by:

$$u(r,\omega) = -\frac{P(\omega)R^3(ik_P - 1/r)\exp(ik_P(r-R))}{4\mu r(1 - ik_P R - k_S^2 R^2/4)}. \tag{10}$$

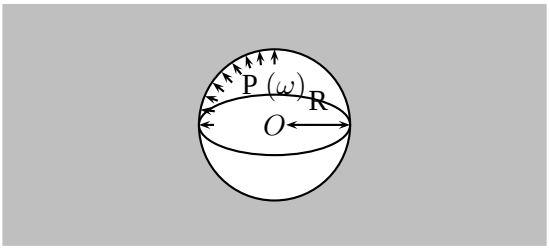


**Figure 3**: **Spherical cavity under internal pressure**

*Accuracy*

The accuracy of the present FMM-accelerated BEM is assessed by comparing numerical results to the known solution (10). The cavity mesh used features 1280 three-noded triangular boundary elements (i.e. 642 nodes and $N = 1926$ DOFs), supporting a continuous, piecewise-linear, interpolation of boundary

displacements. On Figure 4, the real part of the radial displacement is plotted against the radial distance $r/R$ for various normalized frequencies $\eta_P = k_P R/\pi$ (i.e. $\eta_P$ is the number of P wavelengths spanned by the cavity diameter). The numerically-computed displacements are seen to agree very well with the analytical solution. The relative RMS solution errors achieved, shown in Table 1, confirm this assessment. In particular, a good accuracy is obtained for the nearly-static case $\eta_P = 0.01$. This case shows that the FMM can be applied also for low frequencies like the standard BEM (Dangla et al., 2005). Moreover, the results of Table 1 suggest that the accuracy deteriorates if the number of mesh nodes per $S$ wavelength is lower than about $8$. In all subsequent results, the meshes were designed so as to feature at least $10$ nodes per $S$ wavelength.

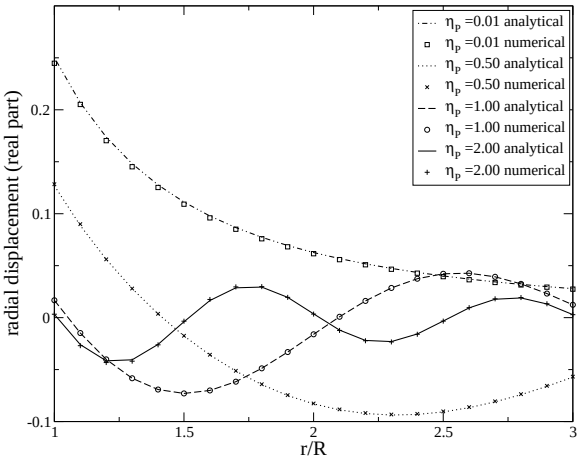


**Figure 4**: **Comparison between numerical FMM and analytical results for normalized frequencies $\eta_P = 0.01, 0.50, 1.00, 2.00$ (Spherical cavity under internal pressure)**

**Table 1**: **RMS solution error on the cavity and in the domain (Spherical cavity under internal pressure)**

| $\eta_P$ | nb nodes $/\lambda_S$ | cavity | domain |
|---|---|---|---|
| 0.01 | 800 | 0.018 | 0.017 |
| 0.50 | 16 | 0.006 | 0.006 |
| 1.00 | 8 | 0.006 | 0.008 |
| 2.00 | 4 | 0.021 | 0.031 |

*Computational efficiency*

The complexity of the classical BEM is $O(N^2)$ per iteration in both CPU time and memory. The theoretical complexities of the one-level and multi-level versions of the FMM are $O(N^{3/2})$and $O(N \log_2 N)$, respectively. These complexity estimates are corroborated by numerical experiments (Figure 5).

**Diffraction of an incident P plane wave by a spherical cavity**

Now, the scattering of an incident plane P wave by the spherical cavity is considered (Figure 6). The configuration is as in the previous example, except that the cavity surface is now traction-free. The incident plane wave propagates along the $z$-direction. The cavity mesh is made of $81920$ triangular boundary elements ($40962$ nodes and $N = 122886$ DOFs). The numerical results are compared to the analytical solution given in Eringen and Suhubi (1975), which incidentally features a typographical error, corrected in Dangla et al. (2005).

The numerical results are computed along radial straight lines emanating from the cavity center in directions ($\theta = 0,\ \pi/4,\ \pi/2,\ 3\pi/4,\ \pi$). Figure 7 shows the real part of the radial displacement computed for the normalized frequencies $\eta_P = 1$ and $4$ against the normalized distance $r/R$. The numerical results obtained using the present FMM-accelerated BEM agree very well with the exact solution for the two

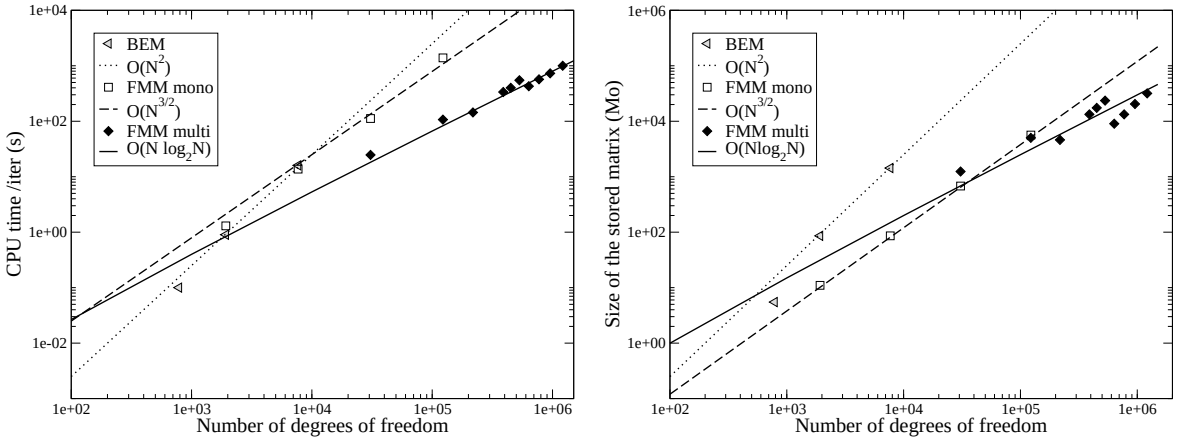


**Figure 5**: **Complexity of the standard BEM, one-level FMM and multi-level FMM, in terms of CPU time (left) and memory (right) (Spherical cavity under internal pressure)**

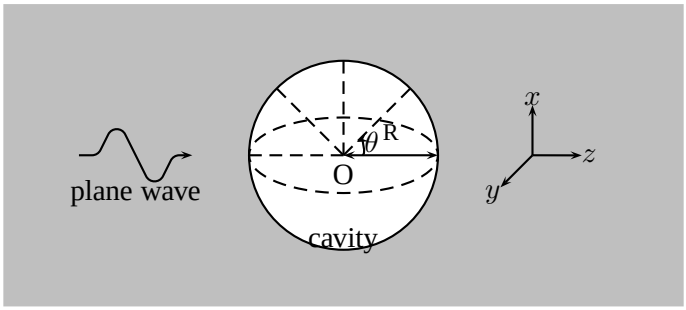


**Figure 6**: **Diffraction of an incident P plane wave by a spherical cavity**

frequencies considered. For the nondimensional frequency $\eta_P = 4$, a solution CPU time of about 2 minutes per iteration (102 GMRES iterations, no preconditioning) was recorded on a single PC (CPU frequency: 3.40 GHz, RAM: 3Mo).

## DIFFRACTION OF ELASTIC WAVES BY A SEMI-SPHERICAL CANYON

The diffraction of incident elastic waves by a semi-spherical canyon is now considered. This phenomenon is a topographic site effect. The chosen geometrical configuration corresponds to a semi-spherical canyon of radius $R$ in an elastic half space (Figure 8). The Poisson's ratio is chosen equal to 0.25. The discretized portion of the free surface is inside a disk of radius $L > R$.

**Diffraction of an incident P plane wave by a semi-spherical canyon**

First, the diffraction of a vertically-travelling P-wave is considered. The canyon mesh is uniform and features 15337 triangular boundary elements (7794 nodes), achieving a minimum of 10 points per $S$ wavelength for all considered frequencies. This problem has been previously investigated by Sánchez-Sesma (1983) using the (semi-analytical) series expansion method. The modulus of the vertical and horizontal displacements, computed using the present FMM, are compared in Figure 9 to corresponding results from Sánchez-Sesma (1983), for two frequencies such that $\eta_P = 0.25,\ 0.50$, and with $L = 3R$ for both studies. A good agreement between the two approaches is observed. On Figure 9, the good adequacy between the results of the two methods can be observed. The main discrepancies occur at points such that $r/R \geq 2$, which are close to the truncation radius $L = 3R$, due to the differences in handling the truncation in both studies. Numerical results for the same problem obtained in Reinoso

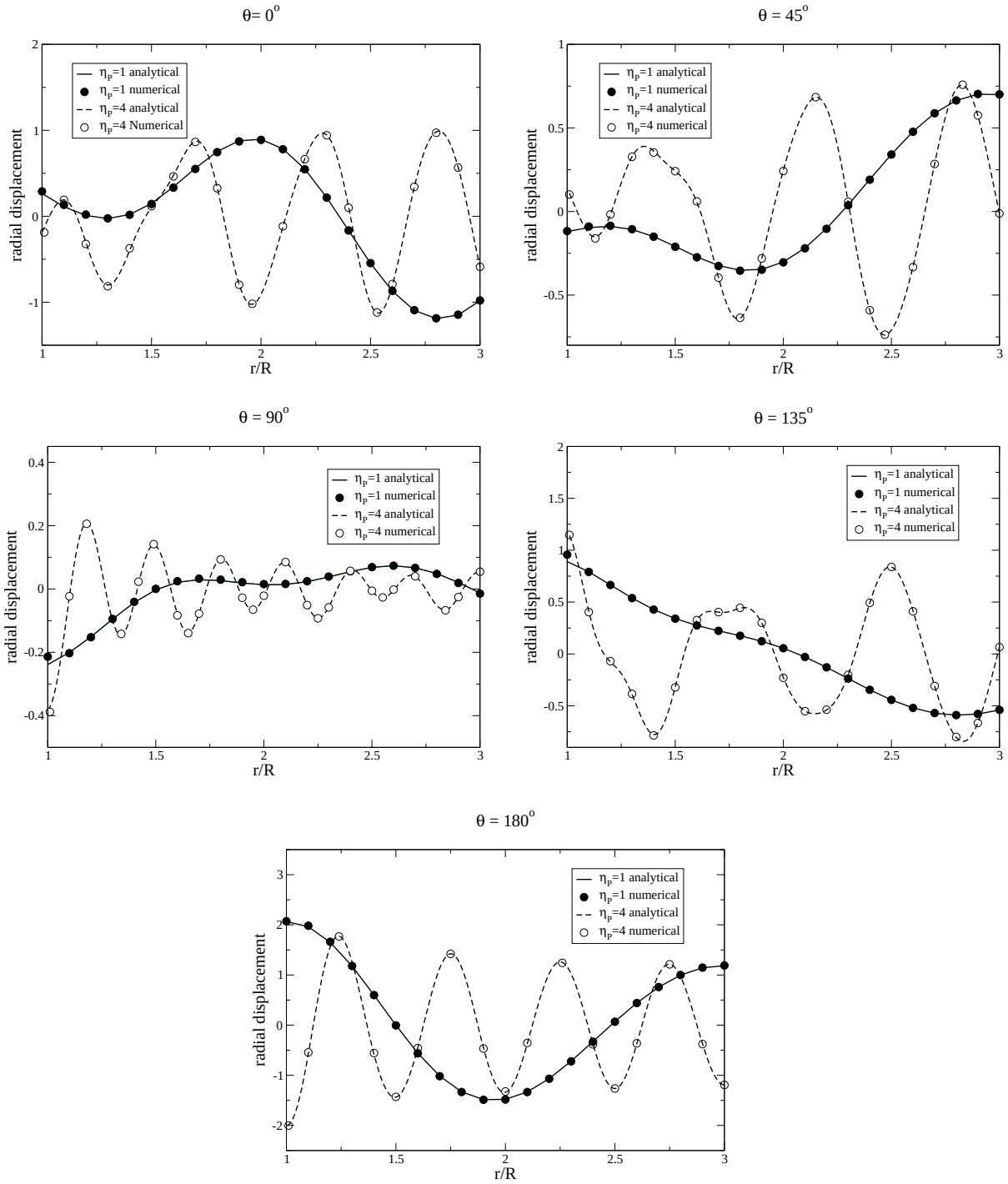


**Figure 7**: **Comparison of the numerical FMM and analytical solutions for normalized frequencies $\eta_P = 1$ and $4$ and for different azimuths $\theta_i$ (Diffraction of an incident P plane wave by a spherical cavity)**

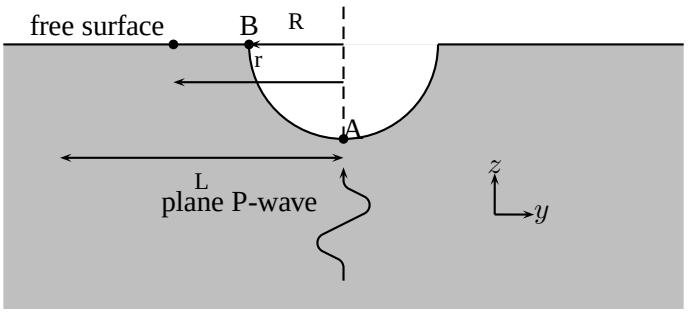


**Figure 8**: **Diffraction of an incident P plane wave by a semi-spherical canyon**

et al. (1997) using the standard BEM elicit similar comments.

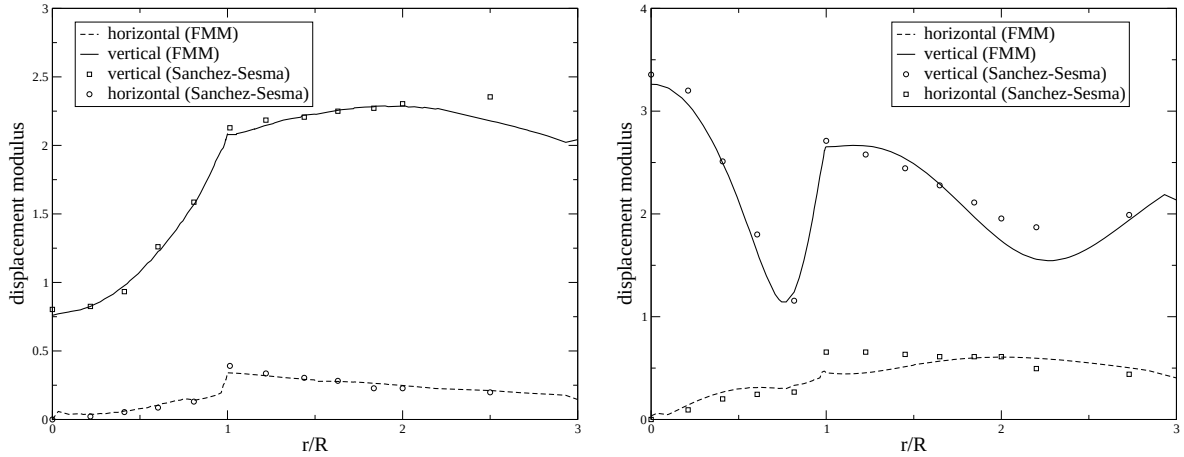


**Figure 9**: **Comparison of the numerical FMM solution and the results of Sánchez-Sesma (1983) for** $\eta_P = 0.25$ **(left) and** $\eta_P = 0.50$ **(right) (**$L = 3R$**) (Diffraction of an incident P plane wave by a semi-spherical canyon)**

The case $\eta_P = 5$ (Figure 10), whose size ($N = 287\ 946$) is well beyond the capabilities of standard BEM, has been solved using the present FMM (86 GMRES iterations, 5 mn CPU time per iteration). In this case, the free surface truncation ($L = 3R$) is seen to generate spurious oscilations for $r/R \geq 2$, and a larger value for $L$ would be advisable (at the cost of increased $N$).

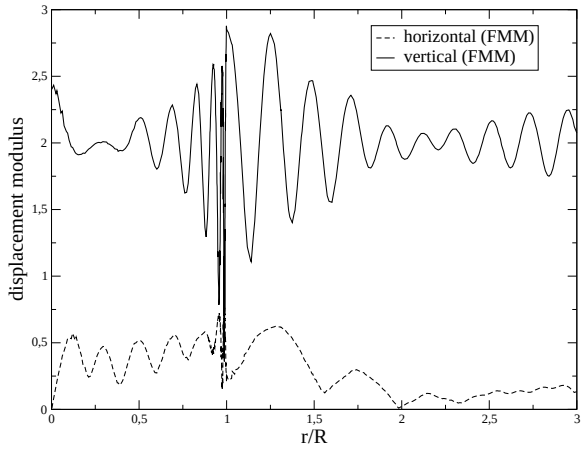


**Figure 10**: **Numerical FMM solution for** $\eta_P = 5$ **(Diffr. incident P plane wave by a semi-spherical canyon)**

*Influence of the size of the discretized free surface*
In Sánchez-Sesma (1983), the size of the discretized free surface is chosen equal to $L = 3R$. A natural issue concerns the selection of the best value of the truncation radius $L$, i.e. the smallest value of $L$ for which the solution is practically insensitive to the free-surface truncation. Taking advantage of the larger problem sizes allowed by the present FMM, this issue is now investigated by means of a parametric study. Of course, the choice of $L$ depends on the size of the region within which the solution is desired to be truncation-independent. Here, the latter is chosen such that $r/R \leq 3$.

On Figure 11, the modulus of both vertical and horizontal displacements are plotted for various truncation radii $L$ ($\eta_P = 0.25$). The sensitivity of the solution to $L$ is seen to be low for $L \geq 5R$. In addition, Table 2 shows the relative difference between the solution computed within the region $r/R \leq 3$ for several truncation radii $L$ and a reference solution obtained for $L = 20R$. These results also suggest that a convergence is achieved for $L \geq 5R$. A similar study has been done in Niu and Dravinski (2003) but limited to $L = 5R$. Here, it can be seen that the proposed size of $L = 3R$ was good but is not enough to have a good precision on the results in the center of the canyon and that best results are obtained using $L = 5R$.

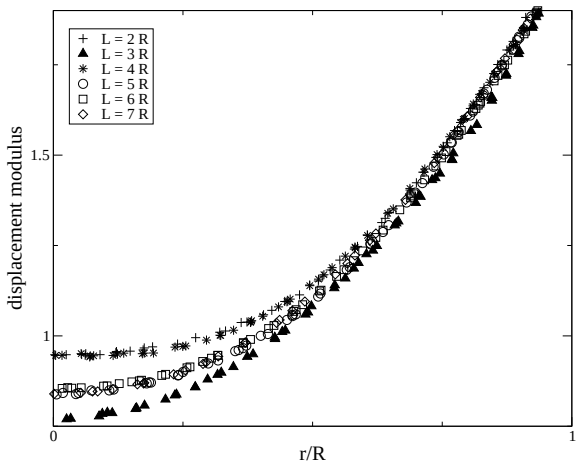


**Figure 11**: **Comparison of the displacement for various truncation radii $L$ (Diffraction of an incident P plane wave by a semi-spherical canyon)**

**Table 2**: **Discrepancy between the reference solution ($L = 20R$) and solutions obtained for various truncation radii $L$ (Diffraction of an incident P plane wave by a semi-spherical canyon)**

| $L$ | $2R$ | $3R$ | $4R$ | $5R$ | $6R$ | $7R$ |
|---|---|---|---|---|---|---|
| error for $r/R \leq 3$ (%) | 3.4 | 2.2 | 3.3 | 1.3 | 1.5 | 1.2 |
| error at point A (%) | 13.1 | 9.7 | 13.1 | 0.8 | 1.9 | 0.7 |

**Diffraction of an incident spherical P wave by a semi-spherical canyon**
The last example deals with the scattering of a point source generated P-wave by a semi-spherical canyon (Figure 12). The geometrical configuration and material parameters used in the previous example are retained. The truncation radius of the free surface is set to $L = 5R$. The point source is located at $(0, 0, z_S)$.

*Influence of the source depth.*
In this example, for various normalized frequencies ($\eta_P = 0.5$ and $0.75$), the influence of the depth of the source is studied. In Figure 14, the amplification factor is plotted for various $z_S$ values ($-2R$, $-3R$, $-4R$ and $-5R$). This amplification factor is defined as the ratio between the modulus of the vertical displacement computed along the topographic irregularity (the canyon in this example) and the

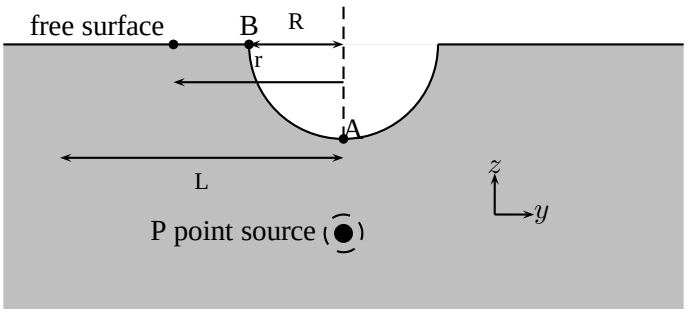


**Figure 12**: **Diffraction of P point source by a semi-spherical canyon**

corresponding value for the free-field. The corresponding points are defined at the free surface on the line between the source and the point considered along the canyon (see Figure 13). This definition permits to consider the spherical behavior of the point source and the free surface effect.

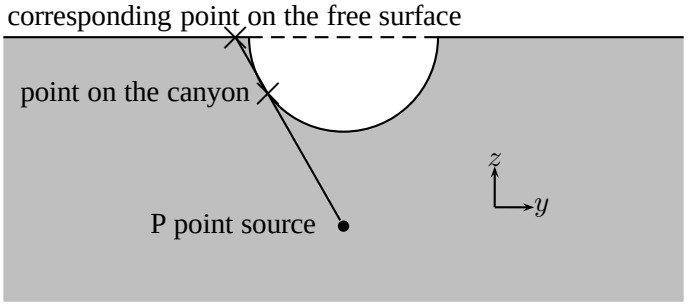


**Figure 13**: **Definition of the amplification factor**

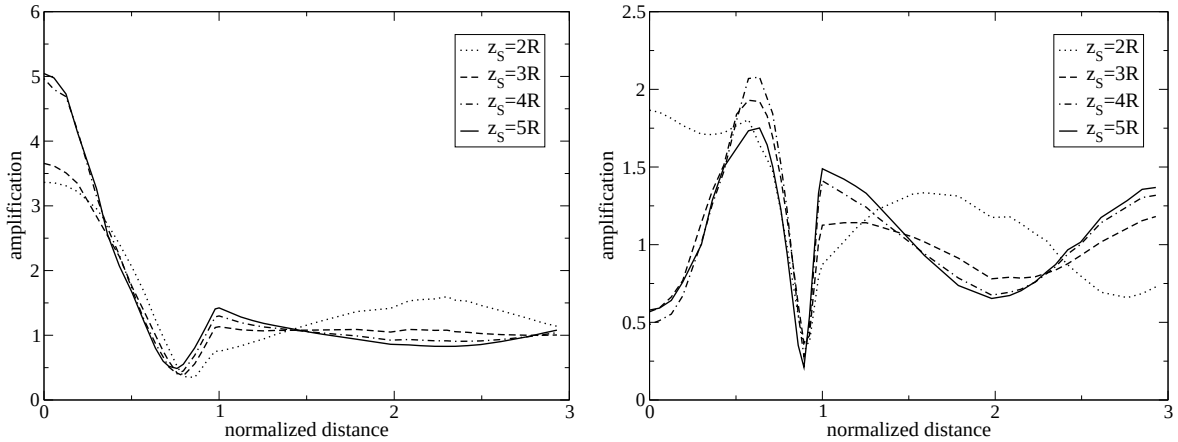


**Figure 14**: **Comparison for various positions of the point source for $\eta_P = 0.5$ (left) and $\eta_P = 0.75$ (right) (Diffraction of an incident spherical P wave by a semi-spherical canyon)**

The first interesting result is that, for large $z_S$ values, the results for a point source are similar to those for a plane wave. This is due to the fact that the point source can be decomposed into a sum of plane waves if the source is far from the canyon (Eringen and Suhubi, 1975). Other ongoing investigations concern the influence of the size of the discretized free surface on this phenomenon.

The second result is the fact that for a large $\eta_P$ value, if the point source is close from the canyon, the effect of the irregularity can be the opposite of the one observed for a plane wave. That is to say that,

for $\eta_P = 0.75$ and $z_S = 2R$, instead of having a decrease of the motion at the center of the canyon, the displacement is amplified. Other ongoing investigations concern the influence of the location of the source in the horizontal plane.

## CONCLUSIONS

In this paper, the fast Multipole Method has been succesfully extended to $3D$ elastodynamics in the frequency domain. Combined with the BEM formulation, it permits to reduce the computational cost in terms of CPU time and memory requirements for the analysis of site effects, and allows to run BEM models of size $N = O(10^6)$ on a ordinary PC computer. As a consequence, more detailed and realistic analyses are now possible in terms of basin size, frequency range, heterogeneities description,.... The comparisons made in this paper (with analytical or previously published results) show the efficiency and accuracy of the present method. The influence of the mesh truncation radius has been studied for the diffraction of a P plane wave by a semi-spherical canyon. Ongoing research work concerns the study of alluvial valleys and detailed comparisons between various numerical approaches for seismic hazard assessment.

## REFERENCES


Abramowitz M and Stegun IA. *Handbook of mathematical functions with formulas, graphs, and mathematical tables*. Dover Publications INC., 1992.

Bard PY and Bouchon M. The 2D resonance of sediment-filled valleys. *Bull. Seism. Soc. Am.*, 75:519–541, 1985.

Bonnet M. *Boundary Integral Equation Method for Solids and Fluids*. Wiley, 1999.

Chaljub E, Capdeville Y and Vilotte JP. Solving elastodynamics in a fluid-solid heterogeneous sphere: a parallel spectral element approximation on non-conforming grids. *J. Comp. Phys.*, 187:457–491, 2003.

Dangla P, Semblat JF, Xiao H and Delépine N. A simple and efficient regularization method for 3D BEM: application to frequency-domain elastodynamics. *Bull. Seism. Soc. Am.*, 95:1916–1927, 2005.

Darve E. The fast multipole method: Numerical implementation. *J. Comp. Phys.*, 160:195–240, 2000.

Eringen AC and Suhubi ES. *Elastodynamics*, volume II-linear theory. Academic Press, 1975.

Fujiwara H. The fast multipole method for solving integral equations of three-dimensional topography and basin problems. *Geophysical Journal International*, 140:198–210, 2000.

Guzina BB and Pak RYS. On the analysis of wave motions in a multi-layered solid. *Quart. J. Mech. Appl. Math.*, 54:13–37, 2001.

Lee VW. 3D diffraction of plane P-, SV- and SH-waves by a hemispherical alluvial valley. *Soil. Dyn. Earthquake Engng.*, 3:133–144, 1984.

Nishimura N. Fast multipole accelerated boundary integral equation methods. *Appl. Mech. Rev.*, 55:299–324, 2002.

Niu Y and Dravinski M. Direct 3D BEM for scattering of elastic waves in a homogenous anisotropic half-space. *Wave Motion*, 38:165–175, 2003.

Reinoso E, Wrobel LC and Power H. Three-dimensional scattering of seismic waves from topographical structures. *Soil. Dyn. Earthquake Engng.*, 16:41–61, 1997.

Sánchez-Sesma FJ. Diffraction of elastic waves by 3D surface irregularities. *Bull. Seism. Soc. Am.*, 73:1621–1636, 1983.

Semblat JF, Paolucci R and Duval AM. Simplified vibratory characterization of alluvial basins. *C. R. Geoscience*, 335:365–370, 2003.

Semblat JF and Bard PY. Models for engineering seismology and earthquake engineering: recent advances and open issues. In $11^{th}$ *Int. Conf. on Computer Methods and Advances in Geomechanics (IACMAG), Torino*. 2005.

Semblat JF, Kham M, Parara E, Bard PY, Makra K and Raptakis D. Site effects: basin geometry vs soil layering. *Soil. Dyn. Earthquake Engng.*, 25:529–538, 2005.

Takahashi T, Nishimura N and Kobayashi S. A fast BIEM for three-dimensional elastodynamics in time domain. *Engineering Analysis with Boundary Elements*, 27:491–506, 2003.